Symmetry control in subscale near-vacuum hohlraums

D. Turnbull, L. F. Berzak Hopkins, S. Le Pape, L. Divol, N. Meezan, O. L. Landen, D. D. Ho, A. Mackinnon, A. B. Zylstra, H. G. Rinderknecht, H. Sio, R. D. Petrasso, J. S. Ross, S. Khan, A. Pak, E. L. Dewald, D. A. Callahan, O. Hurricane, W. W. Hsing, and M. J. Edwards

Citation: Physics of Plasmas **23**, 052710 (2016); doi: 10.1063/1.4950825
View online: http://dx.doi.org/10.1063/1.4950825
View Table of Contents: http://scitation.aip.org/content/aip/journal/pop/23/5?ver=pdfcov
Published by the AIP Publishing

Symmetry control in subscale near-vacuum hohlraums

D. Turnbull,[1,a)] L. F. Berzak Hopkins,[1] S. Le Pape,[1] L. Divol,[1] N. Meezan,[1] O. L. Landen,[1] D. D. Ho,[1] A. Mackinnon,[1,2] A. B. Zylstra,[3,4] H. G. Rinderknecht,[3,1] H. Sio,[3] R. D. Petrasso,[3] J. S. Ross,[1] S. Khan,[1] A. Pak,[1] E. L. Dewald,[1] D. A. Callahan,[1] O. Hurricane,[1] W. W. Hsing,[1] and M. J. Edwards[1]

[1]*National Ignition Facility, LLNL, Livermore, California 94550, USA*
[2]*Linac Coherent Light Source, SLAC, Menlo Park, California 94025, USA*
[3]*Plasma Science and Fusion Center, MIT, Cambridge, Massachusetts 02139, USA*
[4]*Los Alamos National Laboratory, Los Alamos, New Mexico 87545, USA*

(Received 29 March 2016; accepted 3 May 2016; published online 18 May 2016)

Controlling the symmetry of indirect-drive inertial confinement fusion implosions remains a key challenge. Increasing the ratio of the hohlraum diameter to the capsule diameter (case-to-capsule ratio, or CCR) facilitates symmetry tuning. By varying the balance of energy between the inner and outer cones as well as the incident laser pulse length, we demonstrate the ability to tune from oblate, through round, to prolate at a CCR of 3.2 in near-vacuum hohlraums at the National Ignition Facility, developing empirical playbooks along the way for cone fraction sensitivity of various laser pulse epochs. Radiation-hydrodynamic simulations with enhanced inner beam propagation reproduce most experimental observables, including hot spot shape, for a majority of implosions. Specular reflections are used to diagnose the limits of inner beam propagation as a function of pulse length. *Published by AIP Publishing.* [http://dx.doi.org/10.1063/1.4950825]

I. INTRODUCTION

The goal of laser-driven inertial confinement fusion (ICF) is to achieve controlled thermonuclear burn in the laboratory using a large number of high energy lasers to heat and compress a target containing nuclear fuel.[1] A one-dimensional spherical implosion optimizes the fuel compression and burn. To achieve this, indirect-drive ICF uses a high-Z cylindrical cavity (hohlraum) in order to smooth the distribution of radiation seen by a fuel-filled capsule;[2,3] the lasers are fired onto the hohlraum interior surface in order to create a uniform X-ray radiation bath. Most experiments to date at the National Ignition Facility (NIF) have used CH capsules and shaped laser pulses that are $14-22$ ns in duration, which consist of $3-4$ carefully timed shocks.[4–6] A larger number of shocks can (ideally) increase the fuel compression. However, motion of the hohlraum wall during such relatively long laser drives can alter the locations of laser deposition and thereby compromise symmetry control. This motivated the use of a low-Z hohlraum fill gas (typically He with a mass density of $0.96-1.6$ mg/cm^3) to hold back the wall in early experiments.[2,3] However, such fill gases can give rise to unexplained deficits in the laser drive[7] as well as laser–plasma interactions (crossed-beam energy transfer,[8] stimulated Raman scattering, and stimulated Brillouin scattering[9]) that introduce new time-dependent asymmetries. Simulations indicate that the resulting hot spot shape distortions are a key source of performance degradation.[10,11]

An alternative approach to minimize the impact of wall motion is to shorten the laser pulses using high density carbon (HDC) ablators in conjunction with a 2-, 3-, or 4-shock laser drive.[12–15] The denser HDC (3.5 g/cm^3 compared to the 1 g/cm^3 of CH) means an equivalent ablator mass is contained in a much thinner shell through which the first shock propagates more quickly, shortening the overall length of a shock-timed laser pulse. This allows for high-performing 3-shock designs that are only $6-7$ ns in duration, which in turn enables the removal of most of the helium fill gas (down to 0.032 mg/cm^3 in the "near-vacuum" hohlraum, or NVH), reducing the drive deficits and the uncertainties associated with laser-plasma instabilities. Even with these shortened drives, however, the impact of late time laser spot motion and the fidelity with which radiation-hydrodynamic simulations capture that impact remain key uncertainties.

All experiments reported here were conducted at the NIF. The NIF has 192 lasers that are first grouped into quadruplets (or "quads") and subsequently into four cones that each have a different angle of incidence on the hohlraum wall. The 23.5° and 30° incidence "inner" cones illuminate the hohlraum waist to provide equatorial drive onto the capsule, whereas the 44.5° and 50° incidence "outer" cones illuminate the ends of the hohlraum to drive the poles of the capsule. In NVH, the inner and outer cones have the same wavelength (351 nm—the third harmonic, or 3ω, of Nd:YLF), and there is minimal crossed-beam energy transfer,[8] so the ratio of the inner cone incident power to the total power (inner "cone fraction," or CF) is directly adjusted so as to symmetrize the X-ray radiation drive seen by the capsule. The original full scale NVH experiments employed 5.75 mm diameter hohlraums with ≈1 mm inner radius (I.R.) capsules, a standard size that has been used in other campaigns. A round implosion with performance that was well-matched by simulations was demonstrated when using a brief 4.3 ns pulse that launches a single strong shock and achieves a modest $5\times$ convergence.[16] However, maintaining symmetry control while pushing to higher convergence using longer laser pulses proved challenging at this scale[14]

a)Electronic mail: turnbull2@llnl.gov.

due to a dense feature building up in the region between the ablator blowoff and the hohlraum wall, which impedes inner beam propagation at late time, producing an equatorial drive deficit. One approach to mitigating this is known as dynamic beam phasing, wherein the late "pole-hot" drive is compensated for by an earlier "waist-hot" radiation flux in order to obtain a round hot spot at peak compression.[17] However, recent work has shown that radiation flux symmetry swings can degrade performance (even if the hot spot is round at the time of peak emission) due to deviation between the hot spot core shape and the fuel areal density at peak compression, which results in poorly stagnating implosions (residual kinetic energy).[10]

An alternative mitigation strategy is to provide more room for inner beam propagation by increasing the case-to-capsule ratio (CCR). That can be achieved by either increasing the hohlraum diameter, in which case a larger amount of laser energy is needed to reach a given radiation temperature, or reducing the capsule size, which limits performance but also limits the laser power and energy to a level that does not tax the NIF laser too heavily. Taking the latter approach, here we present results in 5.75 mm hohlraums with 844 μm I.R. capsules, which have the same CCR as (and which we therefore dub the "subscale" version of) a 6.72 mm hohlraum with the standard 1 mm I.R. capsule.[17] The results demonstrate the ability to tune from oblate, through round, to prolate at a CCR of 3.2. HYDRA, a radiation-hydrodynamic code that is intended to capture the most important aspects of an indirect-drive ICF implosion,[18] is used to simulate the experiments. By enhancing inner beam propagation in the code, most implosion performance metrics (including hot spot shape) are well-reproduced for a majority of experiments. Two pairs of experiments were carried out in which a cone fraction adjustment during a single epoch of the laser pulse was the only change, in order to derive empirical playbooks for hot spot shape control. Several experiments were carried out with extended laser pulses intended to probe the limits of inner beam propagation and how well the model could predict hot spot shape once the inner cones are significantly impeded. Finally, since an integrated metric such as hot spot shape could be misleading as a means of diagnosing inner beam propagation, inner cone specular reflections that exit the hohlraum—an indicator of inner beam propagation—are analyzed for further insight into hohlraum filling dynamics on each implosion.

II. EXPERIMENTAL SETUP

The six shots reported here employed hohlaum targets with a 5.75 mm diameter, 10.1 mm length, and 3.37 mm laser entrance holes (LEHs), containing 844 μm inner radius, 64 μm-thick un-doped HDC capsules filled with either D_2 or D^3He gas at a mass density in the range of $4-8$ mg/cm^3. The hohlraums were filled with helium gas at the "near-vacuum" level of 0.032 mg/cm^3. The primary diagnostics were X-ray framing cameras that image hot spot emission along polar and equatorial views in order to determine the hot spot shape of the implosion.[19] An illustration of the targets is shown in Fig. 1. The total requested laser power for each of the six experiments is shown in Fig. 2(a), with cone fractions shown in Fig. 2(b).

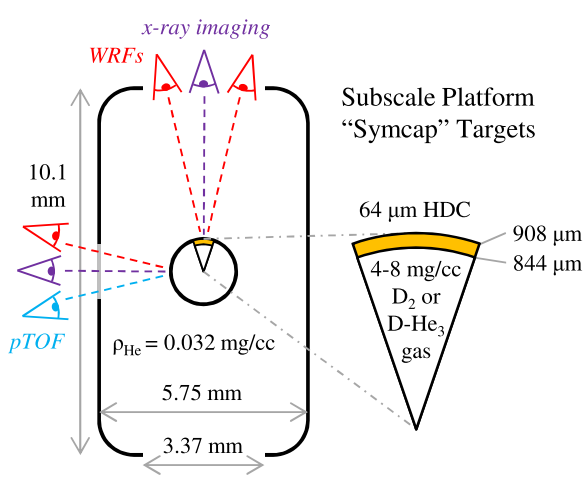

FIG. 1. Description of the experiments. The hohlraums had a 5.75 mm diameter, 10.1 mm length, and 3.37 mm laser entrance holes. The 844 μm I.R. 64 μm-thick undoped HDC capsules were filled with DD or D^3He gas. The experiments were diagnosed with X-ray pinhole imaging, wedged ranged filter proton spectrometers, and a 3ω streaked spectrometer to measure glint.

The inner cone full aperture backscatter (FABS) diagnostic was also fielded.[9] This diagnostic temporally and spectrally resolves light emerging from the target that is close to the 3ω incident laser wavelength and which propagates directly back up a lower hemisphere 30° incidence quad. Though typically used to diagnose backward stimulated Brillouin scattering from the 30° cone, it was recently shown that in NVH, this diagnostic also collects hohlraum wall specular reflections, or "glint," from two upper hemisphere quads.[20,21] The glint from each experiment was analyzed in order to provide feedback about wall motion and the continuity of inner beam propagation during peak power.

Proton spectroscopy was also included on the experiments that used D^3He-filled capsules. Wedged Ranged Filters (WRFs)[22] were fielded at four locations near the pole and three locations near the equator. The WRFs resolve the energy spectrum of the D^3He protons produced by the implosion. The downshift relative to the birth energy of 14.7 MeV can then be used to infer the shell ρR.[23] A proton time-of-flight (pTOF) spectrometer[24] was also fielded near the equator, which is used (in conjunction with the energy spectrum) to determine the times at which the protons are produced.

III. RESULTS AND ANALYSIS

This section describes the results from each of the experiments along with radiation-hydrodynamic simulations. Hot spot symmetry data will be presented chronologically as shown in Fig. 3. Symmetry is quantified using a Legendre polynomial decomposition to describe the size and shape of the implosion; the $l=0$ value P_0 of the 17% emission contour characterizes the size of the hot spot at peak brightness, and higher order modes account for shape distortions. The P_2 mode (often shown normalized by P_0) results from hohlraum drive imbalances between the equatorial and polar

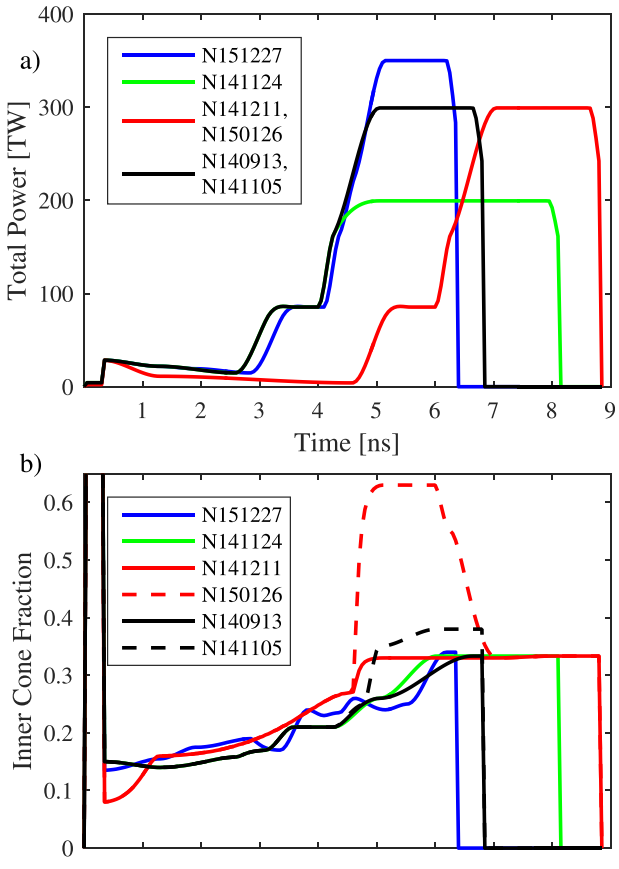

FIG. 2. Requested laser pulses. (a) The total power for each experiment is shown, along with (b) the inner cone fraction. N141105 overlays N140913 except during peak power, and N150126 overlays N141211 except during the second shock and rise to peak power. N141124 and N151227 are very similar to N140913 in terms of cone fraction, but have different pulse lengths and peak powers. The laser always delivered close to the request, with all beams participating on each experiment.

regions and can quickly degrade implosion performance if not well controlled.[10,11] The symmetry data are shown alongside hydrodynamic simulation results.

All simulations were run using HYDRA including a $0.9\times$ multiplier[7] applied during the peak of the drive, and adjusting the inner and outer cone wavelengths as an ad hoc means of enhancing inner beam propagation so as to better reproduce the hot spot implosion shape. It has been clear for some time that, in low gas fill hohlraums, radiation-hydrodynamic models do not accurately predict the radiation flux symmetry during peak power for ignition-relevant implosions. Simulations indicate that a density ridge builds up in the collision region between the hohlraum wall plasma and the ablator blowoff, eventually altering the location of inner cone energy deposition and producing a pole-hot feature in the radiation flux. In simulations, this feature is partially opaque to the inner cone throughout peak power, but radiation flux symmetry can be maintained in simulations early in peak power by steadily increasing the cone fraction (cf. Fig. 2(b)). Simulations also suggest there is a "cliff" near the end of peak power, at which point the inner cone is fully impeded and symmetry control is lost. Since experiments are typically more prolate than simulations (i.e., they are driven "waist-hot"), it was postulated[14,17] that the collision region requires a kinetic treatment in order to be modeled realistically, and that it might therefore be less dense than simulated. Since shorter wavelength light reaches a higher critical density, treating the inner cone as a higher harmonic of the laser fundamental frequency provides a convenient knob to propagate through this dense barrier in the simulations. This rebalances laser energy deposition within the hohlraum without impacting the overall drive, since in both cases, nearly 100% of the laser energy is absorbed within the hohlraum. The inner cone wavelength providing the best match in each case will be shown. In all cases, the outer cone is treated as a longer wavelength (2ω) in order to reduce gold M-band radiation in the simulations so as to be in better agreement with the experimental data. This has a relatively smaller impact on implosion symmetry in the simulations.

A. N140913—A baseline round implosion

The first shot employing the subscale platform was N140913. It used a 3-shock design shown in Figs. 2(a) and 2(b). The resulting shape was very close to round at convergence $\approx 12\times$, with $P_2/P_0 = -8\pm 2\%$ as shown in Fig. 3(a). This was best reproduced in the HYDRA simulations by treating the inner cone as 5ω and the outer cone as 2ω ($5\omega/2\omega$ for short), which established a benchmark from which to tune subsequent implosions. Table I shows that other performance metrics, including X-ray bang time, neutron yield, ion temperature, and burn duration, were well-reproduced by the simulation. The subsequent shots in the campaign all show a similar level of agreement for these parameters. The simulated peak hohlraum radiative temperature—279 eV—excludes the multiplier on peak power that is used in the simulations to match the bang time.

Figure 4 shows the data from the polar WRFs on this shot, plotted with a post-processed proton spectrum from the HYDRA simulation. The first peak near $E \approx 12$ MeV corresponds to protons produced when the merged final shock converges at the center of the capsule ("shock flash"). This was $\approx 500-700$ ps prior to peak compression on these shots, so these protons probe the shell at a radius of $\approx 250\,\mu$m. When the shell stagnates and peak compression is achieved, additional protons are produced that then probe the more highly compressed shell; this accounts for the second, further downshifted, peak in the energy spectrum. The variation in yield at the different WRF locations near the pole is known to be caused by electromagnetic fields near the LEH region.[25] The fact that the peak locations in the simulated spectrum are close to the experimental data indicates that the code is modeling the shell assembly quite well. More detailed proton data analysis (for this shot and others) will be described in a separate paper.

B. N141105—Using peak CF to drive a prolate implosion

A goal of the initial experiments in the campaign was to drive very asymmetric implosions on either side of round, so shot N141105 was designed to drive a prolate implosion by increasing the inner cone fraction during only the peak of the laser pulse. As shown in Fig. 3, this was successfully

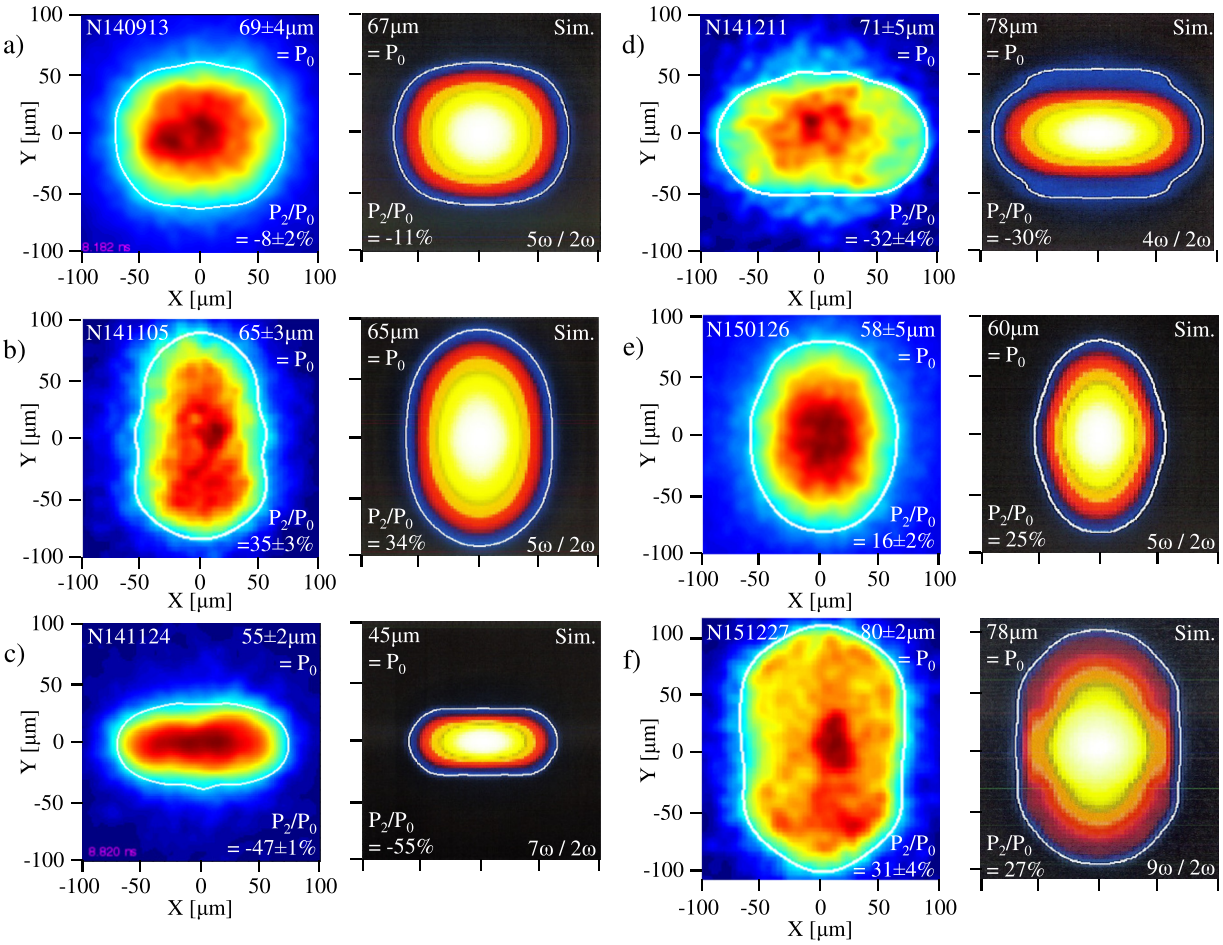

FIG. 3. Implosion shape viewed from equatorial port 90–78 compared to hydrodynamic simulations for each experiment.

achieved, giving $P_2/P_0 = 35\pm3\%$. More importantly, the best simulation match, with near-perfect agreement in terms of both size and shape, used the model that was benchmarked on the previous experiment. This suggests that cone fraction changes can be made within the same overall pulse envelope without compromising the model's ability to reproduce hot spot shape, and that once a set point has been established, it might enable predictable tuning of subsequent implosions.

Along with N140913, this pair of shots also provides an empirical playbook for the effect of a peak cone fraction change on hot spot shape. The average delivered cone fraction during peak power was increased from ≈0.296 to ≈0.369, which changed P_2 from $-5.5\ \mu$m to $+22.8\ \mu$m. The resulting playbook is $\Delta P_2/\Delta CF \approx (3.9\pm0.4)\ \mu$m/%.

We compare the empirical sensitivity of hot spot P_2 to peak cone fraction to the following simple 2D analytic view-factor model.[2,26] We approximate the hohlraum as spatially uniform in radiation temperature T_{rad} except for additional emission at the laser cone spots and lack of emission at the LEH positions. The capsule hot spot P_2 is then the product of the shell distance traveled and the sum of contributing P_2 drive asymmetries from inner and outer beams and the LEH, given by

TABLE I. Shot N140913 performance metrics.

	Data	Simulation
DD yield	$(2.7\pm0.2)\times10^{11}$	3.1×10^{11}
DD T_{ion} (keV)	2.5 ± 0.3	2.4
X-ray bang time (ns)	8.15 ± 0.02	8.1
Burn width (ps)	280 ± 20	280
Peak $T_{rad.}$	286 ± 5	279

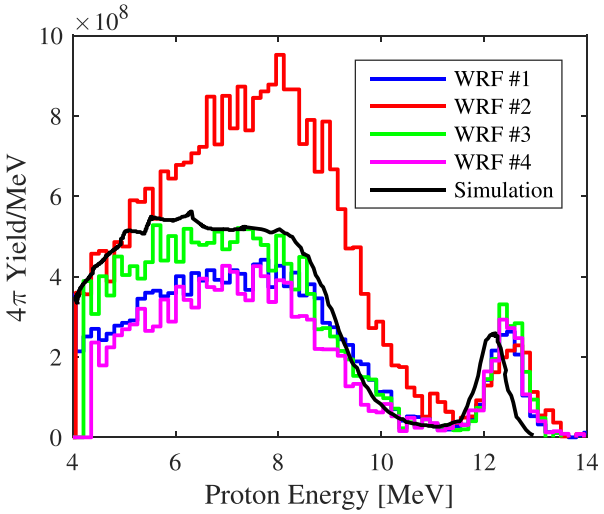

FIG. 4. Simulated versus experimental proton spectrum. The data from the four polar WRFs on N140913 are plotted with HYDRA's post-processed proton spectrum. The energy downshift of each peak is indicative of the shell ρR at shock flash and compression bang time.

$$P_2 = -5(R_0 - P_0) \times \left[\frac{P_2^i S_2^i \epsilon + P_2^o S_2^o (1-\epsilon) - P_2^{LEH} S_2^{LEH} (\Omega_{LEH}/\Omega_W) F}{F+1}\right], \quad (1)$$

where 5 represents the $2n+1$ P_n normalization term, R_0 and P_0 are the average capsule radius at the start of acceleration and at stagnation such that $R_0 - P_0$ is the distance traveled, S_2 is the fraction of P_2 at capsule radius remaining from an applied P_2 at the spot or LEH radius (the smoothing factor), the superscripts i and o refer to inner and outer cones, ϵ is a solid angle weighted peak power cone fraction, and Ω_{LEH} and Ω_W are the solid angles subtended by the LEH and hohlraum wall at the capsule. F is the ratio of recirculating flux to laser produced flux, conveniently related to the hohlraum losses by $F = \alpha/[(1-\alpha) + \Omega_{LEH}/\Omega_W]$, where α is the flux weighted average albedo of the hohlraum at peak power given by Ref. 3 $\alpha = 1 - 0.66/(T_{rad}^{0.7}\tau^{0.46})$, T_{rad} is the radiation temperature (in 10^2 eV) at time $t = 1$ ns after the start of peak laser power, and τ is the duration of peak power drive (in ns). The flux losses to the subscale capsule are ignored in calculating F since it is a small surface area relative to the LEHs, which in turn are small relative to the hohlraum wall.

Taking the derivative of Eq. (1) with respect to the weighted inner cone fraction ϵ, using $P_2^o S_2^o (1-\epsilon) \approx -P_2^i S_2^i \epsilon + P_2^{LEH} S_2^{LEH} (\Omega_{LEH}/\Omega_W) F$ since the data are taken near $P_2 = 0$, yields

$$\Delta P_2 = -5(R_0 - P_0)\left[\frac{P_2^i S_2^i - P_2^{LEH} S_2^{LEH} (\Omega_{LEH}/\Omega_W) F}{F+1}\right]\frac{\Delta\epsilon}{1-\epsilon}. \quad (2)$$

The average smoothing factors are extracted from Fig. 61 in Lindl *et al.*,[2] assuming a trajectory weighted capsule radius of 0.6 mm and assuming that the effective radii or centroid distance of the inner and outer laser spots and LEH are given by their initial values: 2.8, 3.8, and 5.1 mm, respectively. This is a reasonable approximation as the laser spots move in time almost tangentially with respect to the nearest capsule surface. P_2 for the laser spots is defined as the second Legendre moment weighting $0.5(\cos^2(\theta) - 1)$, where θ is the angle subtended with respect to the hohlraum axis by the centroid of the cone spots. For the LEH, we use the solid angle weighted $\theta \approx 12°$. Substituting for all parameters ($R_0 = 800\,\mu$m, $P_0 = 50\,\mu$m, $P_2^i \approx -0.5$ since the inner cone deposits near the P_2 antinode at 90°, $S_2^i = 0.43$, $P_2^{LEH} = 0.94, S_2^{LEH} = 0.35, \Omega_{LEH}/\Omega_W = 0.05, \alpha = 0.75$ and $F = 2.5$ for $T_{rad} = 290$ eV and $t = 1.7$ ns, and $\epsilon = 0.3$) yields $\Delta P_2 = 3.9\,\mu$m/% $\Delta\epsilon$ (or $\approx 3.9\,\mu$m/%CF since ϵ is close to the value of CF in this case), matching the measured value. We can thus say that this pair of NVH behaved as expected from a simple viewfactor perspective.

C. N141124 and N141211—Oblate implosions driven by pulse length extensions

Since another goal of the campaign was to investigate the effect of hohlraum filling on implosion symmetry and the fidelity of hydrodynamic simulations, the subsequent experiments N141124 and N141211 used extended length laser pulses. This allows more time for hohlraum filling, which impedes the inner cone at late time and produces a pole-hot radiation flux onto the capsule according to radiation-hydrodynamic simulations. N141124 extended peak power, but at a level (200 TW) that was 1/3 lower than the original laser pulse so as to better conserve the total laser energy. N141211 instead extended the first shock by 2 ns (lowering the trough power in order to again conserve total laser energy), thereby delaying peak power. Fig. 2(a) shows the pulse shape changes.

Figs. 3(c) and 3(d) show that both implosions were driven significantly oblate, with $P_2/P_0 = -47 \pm 1\%$ on N141124 and $P_2/P_0 = -32 \pm 4\%$ on N141211. The fact that pulse length was the main parameter adjustment on these two shots suggests that laser spot motion induced by hohlraum filling modified the hot spot symmetry. However, the model used to reproduce hot spot shape on the prior two shots no longer gives the best match. On N141124, setting the inner cone wavelength to 7ω is still not enough to match the observed hot spot shape. While this could indicate that inner cone propagation needs to be enhanced still further, it may also simply be due to the fact that the equatorial shape data are saturated; empirically, we have observed that the hot spot shape does not respond linearly to drive aymmetries outside of $P_2/P_0 = \pm 40\%$.

On N141211, the discrepancy goes in the opposite direction, with a $4\omega/2\omega$ model best reproducing the hot spot shape. The most general takeaway is that the perturbations to these experiments (significant pulse length changes and/or the peak power reduction on N141124) were too large for the previously benchmarked model to remain the best predictor of hot spot shape.

D. N150126—An implosion with compensating drive asymmetries

Since the extended foot did in fact drive the implosion oblate on N141211, shot N150126 used the same total power but with an increased cone fraction during the second shock and the rise to peak power (leaving the peak CF unchanged), in order to test the effect of introducing compensating drive asymmetries on performance and our ability to predict hot spot shape. By increasing the delivered cone fraction from $CF = 0.288$ to $CF = 0.512$ (cf. Fig. 2(b)), the hot spot P_2 changed from $-22.7\,\mu$m to $+9.3\,\mu$m. The resulting playbook for this epoch of the laser pulse is $\Delta P_2/\Delta CF \approx (1.43 \pm 0.13)\,\mu$m/%, a little more than 1/3 of the peak cone fraction sensitivity found earlier.

Although Fig. 3 shows only the hot spot shape at peak X-ray emission (X-ray bang time), the shape is actually resolved in time for several hundred ps around bang time using the X-ray framing cameras. It is interesting to note that on this shot, the implosion appeared to be "non-swinging" through bang time, meaning that the hot spot shape appeared relatively static as it converged, as shown in Fig. 5. We generally assume that this is a signature of a well-behaved implosion; although in this case, we believe that the radiation flux is waist-hot during the second shock and rise to peak power, then pole-hot at the end of peak power, even if the end result is a fairly round implosion. N141105 and N141211 were becoming more prolate and oblate at peak

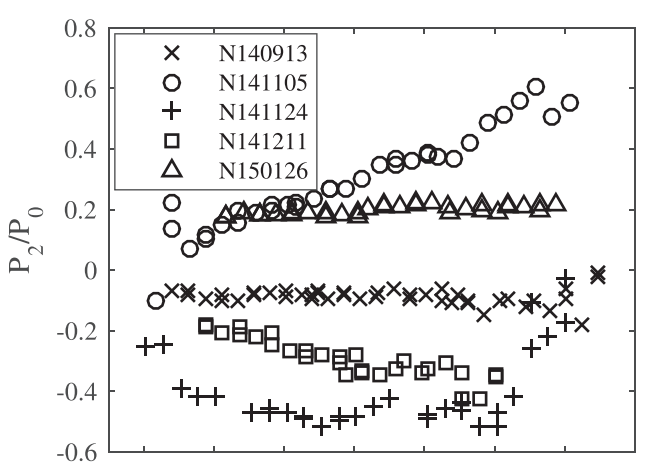

FIG. 5. P_2/P_0 as a function of time. N141105 and N141211 are swinging prolate and oblate, respectively, due to a peak radiation flux asymmetry. N140913 is non-swinging, as is N150126 despite large compensating radiation flux asymmetries. N141124 is also non-swinging, possibly due to saturation.

emission, respectively, consistent with the late time asymmetry on each experiment. N141124, on the other hand, appears static despite the dominant late pole-hot radiation flux, which may provide additional evidence that the shape was saturated and did not fully reflect the drive asymmetry.

E. N151227—A shorter pulse to mitigate symmetry degradation by hohlraum filling

The goal of the final experiment, N151227, was to test a modified 3-shock pulse shape designed to give better performance in a cryogenic DT-layered experiment. Simulations suggested that the original N140913 drive was adequately symmetric for an intermediate convergence ($\approx 12\times$) symcap implosion but not for a more stringent higher convergence ($\approx 27\times$) DT implosion due to a late time hohlraum filling effect. To mitigate this, the duration of peak power was truncated, reducing the overall pulse length to 6.4 ns from 6.85 ns in order to turn off the drive before the onset of the radiation flux asymmetry. To reach a similar hohlraum radiation temperature with the shorter pulse, the amplitude of peak power was increased to 350 TW. The second and third shocks were also slightly delayed to have correct shock timing for a DT-layered implosion. All changes are apparent in Fig. 2(a). The cone fraction trajectory remained very similar to N140913 as shown in Fig. 2(b). The $5\omega/2\omega$ model was used to design the pulse shape, because it had yielded the best agreement with most of the prior shots in the campaign. But as shown in Fig. 3(f), the resulting shape came out quite prolate at $P_2/P_0 = 31 \pm 4\%$, which was ultimately better reproduced using a more aggressive $9\omega/2\omega$ model.

F. Reconciling N140913 and N151227 with the help of glint

As discussed earlier, radiation-hydrodynamic models do not accurately predict the radiation flux symmetry during peak power for ignition-relevant implosions due to inaccurate treatment of a dense feature that builds up between the hohlraum wall plasma and the ablator blowoff. In simulations, this feature is partially opaque to the inner cone during early peak power, but radiation flux symmetry can be maintained at that time by steadily increasing the cone fraction. Simulations also suggest that there is a "cliff" near the end of peak power, at which point the inner cone is fully impeded and symmetry control is lost.

N151227 was specifically designed to avoid the cliff near the end of the laser pulse; not only does a discrepancy remain between nominal $3\omega/3\omega$ HYDRA simulations and the experimental hot spot shape, changing the inner cone wavelength in simulations is much less effective at reproducing hot spot symmetry. A possible explanation is that, early in peak power, the gold and carbon do interpenetrate more freely in experiments than in simulations such that the region remains transparent to the inner cone. The cone fraction increase intended to offset the partial obscuration, then, would instead drive the implosion waist-hot, which could explain the hot spot shape on N151227. In that case, the N140913 hot spot shape could be explained by the fact that the late time cliff does exist in reality and introduces a compensating asymmetry, resulting in a nearly round implosion at peak emission.

The glint data measured by the FABS diagnostic was analyzed for each experiment and provides evidence to bolster this hypothesis. Streaked spectra are shown for four of the shots in Fig. 6, overplotted with the incident inner quad laser pulse. Glint is the feature that is blue-shifted with respect to the incident laser wavelength ($\Delta\lambda < 0$); two of the shots have an additional red-shifted feature that is backward stimulated Brillouin scattering. Glint appears at time zero when the lasers are first incident on the metallic gold wall, and it disappears as the wall ionizes and the density scale length increases. It then reappears during the second and third shocks due to the

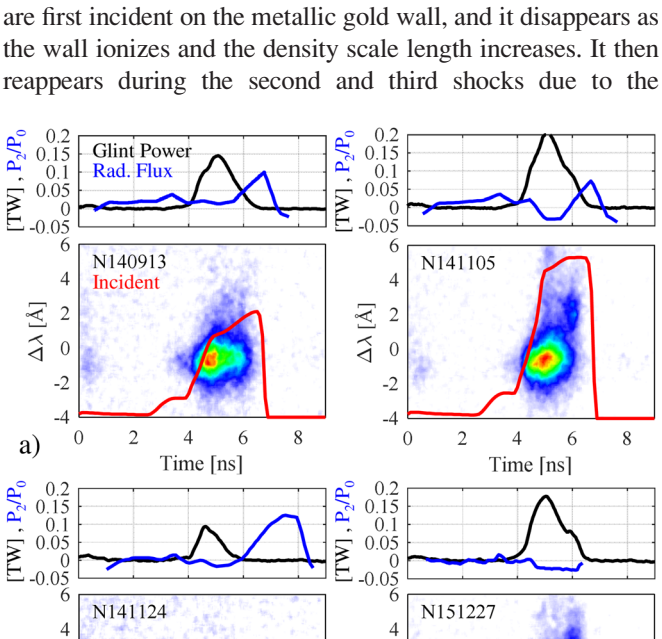

FIG. 6. Glint data from four shots. The streaked spectrum is shown as a function of time, overplotted with the inner cone incident quad pulse shape. The time history is plotted above and compared to the radiation flux symmetry from a $3\omega/3\omega$ HYDRA simulation.

increased power, at which time the reflectivity is on the order of 1%.[20] The glint wavelength is related to the velocity of (and flow rate through) the turning point of the glinting beams ($\approx n_c/4$ where n_c is the critical density for 3ω light);[27] it is quite consistent for all of these shots and suggests that the hohlraum filling dynamics do not substantially change.

N140913, N141105, and N151227 had very similar glint traces in terms of duration. While the glint signals ceased prior to the end of peak power on the former two shots, it lasted for the full laser pulse length on N151227. That is, consistent with HYDRA simulations indicating that N140913 and N141105 suffered from a cliff at late time, which motivated the N151227 pulse shape changes. On N141124, with reduced peak power, the glint signal ends a few hundred picoseconds earlier than the other shots. While this might simply be due to increased absorption in the cooler hohlraum interior, it may also indicate a difference in hohlraum filling due to the large reduction in peak power. Either way, the fact that glint ceases well before the end of the implosion is consistent with late time impeded inner beam propagation and the observed oblate shape.

In fact, the time at which the glint signal disappears on each experiment seems to coincide fairly closely with the time at which HYDRA predicts the onset of radiation flux asymmetry, suggesting that the cliff (which is causing the flux asymmetry) is captured somewhat realistically. This is included in Fig. 6, which for each shot shows the glint time history plotted with the radiation flux symmetry from a nominal $3\omega/3\omega$ HYDRA simulation. A pole-hot radiation drive is positive and a waist-hot radiation drive is negative; the late time positive spike on N140913, N141105, and N141124 results from obstructed inner beam propagation. Similarly, the shots conducted with an extended foot (N141211 and N150126), which are not shown, exhibited very weak glint signals that ended well before the end of the laser pulses. The strong pole-hot feature is absent from the N151227 simulation due to the shorter pulse length.

Changing the inner cone wavelength in simulations is inherently limited because it is a single knob that is partially suppressing both the early peak power mild obscuration and the late peak power cliff. This could explain why a given model works locally (i.e., benchmarking to N140913 allowed predictable tuning of N141105) but not when the balance of the two effects changes (i.e., when the cliff is removed as in N151227 or exacerbated with a longer pulse length). In this scenario, the implosion N140913 was close to round because the drive included compensating asymmetries during peak power. It appeared well-behaved in that the shape was not changing at peak convergence, but N150126 revealed that it is possible to drive much larger compensating asymmetries and still obtains a non-swinging hot spot.

Having shown that cone fraction changes alter implosion symmetry in line with expectations, and having derived empirical playbooks for symmetry tuning using cone fraction at this scale, we can use those playbooks to symmetrize the N151227 pulse shape design. The delivered cone fraction during peak power on N151227 increased from about $CF = 0.235$ to $CF = 0.325$ at the end of the pulse, with an average peak cone fraction of $CF \approx 0.279$. Since N151227 had $P_2 = 24.8$ μm, our empirical playbook suggests a peak cone fraction of $CF \approx 0.215$ would result in a round hot spot at bang time.

IV. CONCLUSIONS

In 5.75 mm diameter indirect-drive ICF near-vacuum hohlraums, a case-to-capsule ratio of 3.2 is an attractive scale because it provides enough room for inner beam propagation (thus allowing a symmetric radiation flux) while reaching high radiative temperatures and while keeping the fuel adiabat low enough to obtain significant neutron yields. We have demonstrated the ability to tune from oblate to prolate at this scale through cone fraction and pulse length changes. In several instances, changing the wavelengths of the inner and outer cones in simulations provides a convenient method of enhancing inner beam propagation in order to reproduce measured hot spot symmetry. After benchmarking such a model on existing experimental data, it is especially useful for making pure cone fraction changes. However, such an approach may not work in the absence of a late-time stagnation feature, as was the case on N151227. The empirical playbooks derived here—$\Delta P_2/\Delta CF \approx (3.9 \pm 0.4)$ μm/% at the peak and $\Delta P_2/\Delta CF \approx (1.43 \pm 0.13)$ μm/% during the second shock and rise to peak—could be used to correct the cone fraction trajectory of N151227 in order to design an implosion that is driven symmetrically throughout the entire pulse duration.

ACKNOWLEDGMENTS

This work was performed under the auspices of the U.S. Department of Energy by Lawrence Livermore National Laboratory under Contract No. DE-AC52-07NA27344. We thank the NIF facility, target fabrication, and diagnostic analysis groups for enabling a successful series of experiments.

APPENDIX: ADDITIONAL SHOT PERFORMANCE METRICS

For the sake of posterity, key experimental parameters for each shot are included in Table II. The first three experiments and N150126 used capsules that were filled with a

TABLE II. Shot performance metrics.

	N140913	N141105	N141124	N141211	N150126	N151227
DD yield (10^{11})	2.7 ± 0.2	2.3 ± 0.2	1.6 ± 0.2	43 ± 3	2.0 ± 0.3	43 ± 3
DD T_{ion} (keV)	2.5 ± 0.3	2.5 ± 0.2	2.3 ± 0.2	2.6 ± 0.1	2.6 ± 0.1	2.6 ± 0.1
X-ray BT (ns)	8.15 ± 0.02	8.11 ± 0.05	8.82 ± 0.02	10.16 ± 0.02	10.1 ± 0.05	8.31 ± 0.05
Burn width (ps)	280 ± 20	230 ± 40	260 ± 60	260 ± 30	280 ± 40	290 ± 40
Dante $T_{rad.}$ (eV)	286 ± 5	282 ± 5	261 ± 5	279 ± 5	279 ± 5	293 ± 5

mixture of 30% atomic fraction deuterium and 70% atomic fraction helium-3. The remaining, higher yield, experiments used capsules filled with 100% deuterium.

[1]J. Nuckolls, A. Thiessen, L. Wood, and G. Zimmerman, "Laser compression of matter to super-high densities: thermonuclear (CTR) applications," Nature **239**, 139–142 (1972).

[2]J. Lindl, "Development of the indirect-drive approach to inertial confinement fusion and the target physics basis for ignition and gain," Phys. Plasmas **2**, 3933–4024 (1995).

[3]J. Lindl, P. Amendt, R. Berger, S. Glendinning, S. Glenzer, S. Haan, R. Kauffman, O. Landen, and L. Suter, "The physics basis for ignition using indirect-drive targets on the National Ignition Facility," Phys. Plasmas **11**, 339–490 (2004).

[4]T. Dittrich, O. Hurricane, D. Callahan, E. Dewald, T. Doppner, D. Hinkel, L. B. Hopkins, S. L. Pape, T. Ma, J. Milovich, J. Moreno, P. Patel, H.-S. Park, B. Remington, and J. Salmonson, "Design of a high-foot high-adiabat ICF capsule for the National Ignition Facility," Phys. Rev. Lett. **112**, 055002 (2014).

[5]S. Haan, J. Lindl, D. Callahan, D. Clark, J. Salmonson, B. Hammel, L. Atherton, R. Cook, M. Edwards, S. Glenzer, A. Hamza, S. Hatchett, M. Herrmann, D. Hinkel, D. Ho, H. Huang, O. Jones, J. Kline, G. Kyrala, O. Landen, B. MacGowan, M. Marinak, D. Meyerhofer, J. Milovich, K. Moreno, E. Moses, D. Munro, A. Nikroo, R. Olson, K. Peterson, S. Pollaine, J. Ralph, H. Robey, B. Spears, P. Springer, L. Suter, C. Thomas, R. Town, R. Vesey, S. Weber, H. Wilkens, and D. Wilson, "Point design targets, specifications, and requirements for the 2010 ignition campaign on the National Ignition Facility," Phys. Plasmas **18**, 051001 (2011).

[6]O. A. Hurricane, D. A. Callahan, D. T. Casey, P. M. Celliers, C. Cerjan, E. L. Dewald, T. R. Dittrich, T. Doeppner, D. E. Hinkel, L. F. B. Hopkins, J. L. Kline, S. Le Pape, T. Ma, A. G. MacPhee, J. L. Milovich, A. Pak, H. S. Park, P. K. Patel, B. A. Remington, J. D. Salmonson, P. T. Springer, and R. Tommasini, "Fuel gain exceeding unity in an inertially confined fusion implosion," Nature **506**, 343 (2014).

[7]O. S. Jones, C. J. Cerjan, M. M. Marinak, J. L. Milovich, H. F. Robey, P. T. Springer, L. R. Benedetti, D. L. Bleuel, E. J. Bond, D. K. Bradley, D. A. Callahan, J. A. Caggiano, P. M. Celliers, D. S. Clark, S. M. Dixit, T. Doppner, R. J. Dylla-Spears, E. G. Dzentitis, D. R. Farley, S. M. Glenn, S. H. Glenzer, S. W. Haan, B. J. Haid, C. A. Haynam, D. G. Hicks, B. J. Kozioziemski, K. N. LaFortune, O. L. Landen, E. R. Mapoles, A. J. MacKinnon, J. M. McNaney, N. B. Meezan, P. A. Michel, J. D. Moody, M. J. Moran, D. H. Munro, M. V. Patel, T. G. Parham, J. D. Sater, S. M. Sepke, B. K. Spears, R. P. J. Town, S. V. Weber, K. Widmann, C. C. Widmayer, E. A. Williams, L. J. Atherton, M. J. Edwards, J. D. Lindl, B. J. MacGowan, L. J. Suter, R. E. Olson, H. W. Herrmann, J. L. Kline, G. A. Kyrala, D. C. Wilson, J. Frenje, T. R. Boehly, V. Glebov, J. P. Knauer, A. Nikroo, H. Wilkens, and J. D. Kilkenny, "A high-resolution integrated model of the national ignition campaign cryogenic layered experiments," Phys. Plasmas **19**, 056315 (2012).

[8]P. Michel, L. Divol, E. A. Williams, C. A. Thomas, D. A. Callahan, S. Weber, S. W. Haan, J. D. Salmonson, N. B. Meezan, O. L. Landen, S. Dixit, D. E. Hinkel, M. J. Edwards, B. J. MacGowan, J. D. Lindl, S. H. Glenzer, and L. J. Suter, "Energy transfer between laser beams crossing in ignition hohlraums," Phys. Plasmas **16**, 042702 (2009).

[9]J. D. Moody, P. Datte, K. Krauter, E. Bond, P. A. Michel, S. H. Glenzer, L. Divol, C. Niemann, L. Suter, N. Meezan, B. J. MacGowan, R. Hibbard, R. London, J. Kilkenny, R. Wallace, J. L. Kline, K. Knittel, G. Frieders, B. Golick, G. Ross, K. Widmann, J. Jackson, S. Vernon, and T. Clancy, "Backscatter measurements for NIF ignition targets (invited)," Rev. Sci. Instrum. **81**, 10D921 (2010).

[10]A. Kritcher, R. Town, D. Bradley, D. Clark, B. Spears, O. Jones, S. Haan, P. Springer, J. Lindl, R. Scott, D. Callahan, M. Edwards, and O. Landen, "Metrics for long wavelength asymmetries in inertial confinement fusion implosions on the National Ignition Facility," Phys. Plasmas **21**, 042708 (2014).

[11]D. S. Clark, M. M. Marinak, C. R. Weber, D. C. Eder, S. W. Haan, B. A. Hammel, D. E. Hinkel, O. S. Jones, J. L. Milovich, P. K. Patel, H. F. Robey, J. D. Salmonson, S. M. Sepke, and C. A. Thomas, "Radiation hydrodynamics modeling of the highest compression inertial confinement fusion ignition experiment from the national ignition campaign," Phys. Plasmas **22**, 022703 (2015).

[12]A. J. MacKinnon, N. B. Meezan, J. S. Ross, S. Le Pape, L. B. Hopkins, L. Divol, D. Ho, J. Milovich, A. Pak, J. Ralph, T. Doeppner, P. K. Patel, C. Thomas, R. Tommasini, S. Haan, A. G. MacPhee, J. McNaney, J. Caggiano, R. Hatarik, R. Bionta, T. Ma, B. Spears, J. R. Rygg, L. R. Benedetti, R. P. J. Town, D. Bradley, E. L. Dewald, D. Fittinghoff, O. S. Jones, H. Robey, J. D. Moody, S. Khan, D. A. Callahan, A. Hamza, J. Biener, P. M. Celliers, D. G. Braun, D. J. Erskine, S. T. Prisbrey, R. J. Wallace, B. Kozioziemski, R. Dylla-Spears, J. Sater, G. Collins, E. Storm, W. Hsing, O. Landen, J. L. Atherton, J. D. Lindl, M. Edwards, J. A. Frenje, M. Gatu-Johnson, C. K. Li, R. Petrasso, H. Rinderknecht, M. Rosenberg, F. H. Seguin, A. Zylstra, J. P. Knauer, G. Grim, N. Guler, F. Merrill, R. Olson, G. A. Kyrala, J. D. Kilkenny, A. Nikroo, K. Moreno, D. E. Hoover, C. Wild, and E. Werner, "High-density carbon ablator experiments on the National Ignition Facility," Phys. Plasmas **21**, 056318 (2014).

[13]L. F. Berzak Hopkins, N. B. Meezan, S. Le Pape, L. Divol, A. J. Mackinnon, D. D. Ho, M. Hohenberger, O. S. Jones, G. Kyrala, J. L. Milovich, A. Pak, J. E. Ralph, J. S. Ross, L. R. Benedetti, J. Biener, R. Bionta, E. Bond, D. Bradley, J. Caggiano, D. Callahan, C. Cerjan, J. Church, D. Clark, T. Döppner, R. Dylla-Spears, M. Eckart, D. Edgell, J. Field, D. N. Fittinghoff, M. Gatu Johnson, G. Grim, N. Guler, S. Haan, A. Hamza, E. P. Hartouni, R. Hatarik, H. W. Herrmann, D. Hinkel, D. Hoover, H. Huang, N. Izumi, S. Khan, B. Kozioziemski, J. Kroll, T. Ma, A. MacPhee, J. McNaney, F. Merrill, J. Moody, A. Nikroo, P. Patel, H. F. Robey, J. R. Rygg, J. Sater, D. Sayre, M. Schneider, S. Sepke, M. Stadermann, W. Stoeffl, C. Thomas, R. P. J. Town, P. L. Volegov, C. Wild, C. Wilde, E. Woerner, C. Yeamans, B. Yoxall, J. Kilkenny, O. L. Landen, W. Hsing, and M. J. Edwards, "First high-convergence cryogenic implosion in a near-vacuum hohlraum," Phys. Rev. Lett. **114**, 175001 (2015).

[14]N. B. Meezan, L. F. Berzak Hopkins, S. Le Pape, L. Divol, A. J. MacKinnon, T. Dppner, D. D. Ho, O. S. Jones, S. F. Khan, T. Ma, J. L. Milovich, A. E. Pak, J. S. Ross, C. A. Thomas, L. R. Benedetti, D. K. Bradley, P. M. Celliers, D. S. Clark, J. E. Field, S. W. Haan, N. Izumi, G. A. Kyrala, J. D. Moody, P. K. Patel, J. E. Ralph, J. R. Rygg, S. M. Sepke, B. K. Spears, R. Tommasini, R. P. J. Town, J. Biener, R. M. Bionta, E. J. Bond, J. A. Caggiano, M. J. Eckart, M. Gatu Johnson, G. P. Grim, A. V. Hamza, E. P. Hartouni, R. Hatarik, D. E. Hoover, J. D. Kilkenny, B. J. Kozioziemski, J. J. Kroll, J. M. McNaney, A. Nikroo, D. B. Sayre, M. Stadermann, C. Wild, B. E. Yoxall, O. L. Landen, W. W. Hsing, and M. J. Edwards, "Cryogenic tritium-hydrogen-deuterium and deuterium-tritium layer implosions with high density carbon ablators in near-vacuum hohlraums," Phys. Plasmas **22**, 062703 (2015).

[15]J. S. Ross, D. Ho, J. Milovich, T. Döppner, J. McNaney, A. G. MacPhee, A. Hamza, J. Biener, H. F. Robey, E. L. Dewald, R. Tommasini, L. Divol, S. Le Pape, L. B. Hopkins, P. M. Celliers, O. Landen, N. B. Meezan, and A. J. Mackinnon, "High-density carbon capsule experiments on the National Ignition Facility," Phys. Rev. E **91**, 021101 (2015).

[16]S. Le Pape, L. Divol, L. B. Hopkins, A. Mackinnon, N. B. Meezan, D. Casey, J. Frenje, H. Herrmann, J. McNaney, T. Ma, K. Widmann, A. Pak, G. Grimm, J. Knauer, R. Petrasso, A. Zylstra, H. Rinderknecht, M. Rosenberg, M. Gatu-Johnson, and J. D. Kilkenny, "Observation of a reflected shock in an indirectly driven spherical implosion at the National Ignition Facility," Phys. Rev. Lett. **112**, 225002 (2014).

[17]L. F. Berzak Hopkins, S. Le Pape, L. Divol, N. B. Meezan, A. J. Mackinnon, D. D. Ho, O. S. Jones, S. Khan, J. L. Milovich, J. S. Ross, P. Amendt, D. Casey, P. M. Celliers, A. Pak, J. L. Peterson, J. Ralph, and J. R. Rygg, "Near-vacuum hohlraums for driving fusion implosions with high density carbon ablators," Phys. Plasmas **22**, 056318 (2015).

[18]M. M. Marinak, G. D. Kerbel, N. A. Gentile, O. Jones, D. Munro, S. Pollaine, T. R. Dittrich, and S. W. Haan, "Three-dimensional hydra simulations of National Ignition Facility targets," Phys. Plasmas **8**, 2275 (2001).

[19]G. A. Kyrala, S. Dixit, S. Glenzer, D. Kalantar, D. Bradley, N. Izumi, N. Meezan, O. L. Landen, D. Callahan, S. V. Weber, J. P. Holder, S. Glenn, M. J. Edwards, P. Bell, J. Kimbrough, J. Koch, R. Prasad, L. Suter, J. L. Kline, and J. Kilkenny, "Measuring symmetry of implosions in cryogenic *Hohlraums* at the NIF using gated x-ray detectors (invited)," Rev. Sci. Instrum. **81**, 10E316 (2010).

[20]D. Turnbull, P. Michel, J. E. Ralph, L. Divol, J. S. Ross, L. F. Berzak Hopkins, A. L. Kritcher, D. E. Hinkel, and J. D. Moody, "Multibeam seeded brillouin sidescatter in inertial confinement fusion experiments," Phys. Rev. Lett. **114**, 125001 (2015).

[21]D. Turnbull, J. Moody, P. Michel, J. Ralph, and L. Divol, "Polarimetry of uncoupled light on the NIF," Rev. Sci. Instrum. **85**, 11E603 (2014).

[22]A. B. Zylstra, J. A. Frenje, F. H. Sguin, M. J. Rosenberg, H. G. Rinderknecht, M. G. Johnson, D. T. Casey, N. Sinenian, M. J.-E. Manuel, C. J. Waugh, H. W. Sio, C. K. Li, R. D. Petrasso, S. Friedrich, K. Knittel, R. Bionta, M. McKernan, D. Callahan, G. W. Collins, E. Dewald, T. Dppner, M. J. Edwards, S. Glenzer, D. G. Hicks, O. L. Landen, R. London, A. Mackinnon, N. Meezan, R. R. Prasad, J. Ralph, M. Richardson, J. R. Rygg, S. Sepke, S. Weber, R. Zacharias, E. Moses, J. Kilkenny, A. Nikroo, T. C. Sangster, V. Glebov, C. Stoeckl, R. Olson, R. J. Leeper, J. Kline, G. Kyrala, and D. Wilson, "Charged-particle spectroscopy for diagnosing shock ρR and strength in NIF implosions," Rev. Sci. Instrum. **83**, 10D901 (2012).

[23]A. B. Zylstra, J. A. Frenje, F. H. Sguin, D. G. Hicks, E. L. Dewald, H. F. Robey, J. R. Rygg, N. B. Meezan, M. J. Rosenberg, H. G. Rinderknecht, S. Friedrich, R. Bionta, R. Olson, J. Atherton, M. Barrios, P. Bell, R. Benedetti, L. Berzak Hopkins, R. Betti, D. Bradley, D. Callahan, D. Casey, G. Collins, S. Dixit, T. Dppner, D. Edgell, M. J. Edwards, M. Gatu Johnson, S. Glenn, S. Glenzer, G. Grim, S. Hatchett, O. Jones, S. Khan, J. Kilkenny, J. Kline, J. Knauer, A. Kritcher, G. Kyrala, O. Landen, S. LePape, C. K. Li, J. Lindl, T. Ma, A. Mackinnon, A. Macphee, M. J.-E. Manuel, D. Meyerhofer, J. Moody, E. Moses, S. R. Nagel, A. Nikroo, A. Pak, T. Parham, R. D. Petrasso, R. Prasad, J. Ralph, M. Rosen, J. S. Ross, T. C. Sangster, S. Sepke, N. Sinenian, H. W. Sio, B. Spears, P. Springer, R. Tommasini, R. Town, S. Weber, D. Wilson, and R. Zacharias, "The effect of shock dynamics on compressibility of ignition-scale National Ignition Facility implosions," Phys. Plasmas **21**, 112701 (2014).

[24]H. G. Rinderknecht, M. G. Johnson, A. B. Zylstra, N. Sinenian, M. J. Rosenberg, J. A. Frenje, C. J. Waugh, C. K. Li, F. H. Sguin, R. D. Petrasso, J. R. Rygg, J. R. Kimbrough, A. MacPhee, G. W. Collins, D. Hicks, A. Mackinnon, P. Bell, R. Bionta, T. Clancy, R. Zacharias, T. Dppner, H. S. Park, S. LePape, O. Landen, N. Meezan, E. I. Moses, V. U. Glebov, C. Stoeckl, T. C. Sangster, R. Olson, J. Kline, and J. Kilkenny, "A novel particle time of flight diagnostic for measurements of shock- and compression-bang times in D^3He and DT implosions at the NIF," Rev. Sci. Instrum. **83**, 10D902 (2012).

[25]C. K. Li, A. B. Zylstra, J. A. Frenje, F. H. Seguin, N. Sinenian, R. D. Petrasso, P. A. Amendt, R. Bionta, S. Friedrich, G. W. Collins, E. Dewald, T. Doeppner, S. H. Glenzer, D. G. Hicks, O. L. Landen, J. D. Kilkenny, A. J. Mackinnon, N. Meezan, J. Ralph, J. R. Rygg, J. Kline, and G. Kyrala, "Observation of strong electromagnetic fields around laser-entrance holes of ignition-scale hohlraums in inertial-confinement fusion experiments at the National Ignition Facility," New J. Phys. **15**, 025040 (2013).

[26]O. L. Landen, P. A. Amendt, L. J. Suter, R. E. Turner, S. G. Glendinning, S. W. Haan, S. M. Pollaine, B. A. Hammel, M. Tabak, M. D. Rosen, and J. D. Lindl, "A simple time-dependent analytic model of the P_2 asymmetry in cylindrical hohlraums," Phys. Plasmas **6**, 2137–2143 (1999).

[27]T. Dewandre, J. Albritton, and E. Williams, "Doppler shift of laser light reflected from expanding plasmas," Phys. Fluids **24**, 528 (1981).